Spatial signature of white matter hyperintensities in stroke patients

Markus D. Schirmer[1,2,3], Anne-Katrin Giese[1,4], Panagiotis Fotiadis[1], Mark R. Etherton[1], Lisa Cloonan[1], Anand Viswanathan[1], Steven M. Greenberg[1], Ona Wu[5], Natalia S. Rost[1]

[1] Department of Neurology, Massachusetts General Hospital, Harvard Medical School, Boston MA, USA

[2] Computer Science and Artificial Intelligence Lab, MIT, USA

[3] Department of Population Health Sciences, German Centre for Neurodegenerative Diseases (DZNE), Germany

[4] Program in Medical and Population Genetics, Broad Institute of MIT and Harvard, Cambridge MA, USA

[5] Athinoula A. Martinos Center for Biomedical Imaging, Department of Radiology, Massachusetts General Hospital, Charlestown, MA

*** Correspondence:**
Dr. Markus D. Schirmer (mschirmer1@mgh.harvard.edu)

Keywords: acute ischemic stroke, white matter hyperintensity, spatial, vascular territory, template

Abstract

White matter hyperintensity (WMH) is a common phenotype across a variety of neurological diseases, particularly in acute ischemic stroke patients. So far, vascular territory dependent variation in WMH burden has not been identified. Here, we investigate the spatial specificity of WMH burden in a cohort of 882 acute ischemic stroke patients. We create an age-appropriate high-resolution brain template on which vascular territories are defined. After spatial normalization this allows for discrimination between WMH volume within each subject's anterior, medial and posterior cerebral artery territories. Using a general linear model, we demonstrate that age, history of smoking and hypertensive status affects the territorial, relative to global, WMH burden, while accounting for the size differences of each territory. Differentiating between anterior (anterior and medial cerebral artery) and posterior territory (posterior cerebral artery), we show that age does not alter the relative distribution of disease burden, while history of smoking and hypertensive status lead to a relative increase of WMH burden within the anterior territory. These results establish the spatial specificity of WMH distribution in relation to vascular territory and risk factor exposure in AIS patients and offers new insights into the underlying pathology.

1 Introduction

White matter hyperintensity (WMH) is an important and widely studied radiographic phenotype (Debette and Markus, 2010). Even though WMH burden has been linked to both incidence and outcomes of stroke (Kuller et al., 2004), spatial specificity of WMH has not been fully explored. WMH is commonly assessed on Fluid Attenuated Inverse Recovery (FLAIR) magnetic resonance (MR) images and total WMH burden can be summarized as WMH volume (WMHv) (Debette and Markus, 2010; Giese et al., 2017; Kuller et al., 2004). Importantly, it has been shown, that WMHv presents an accurate and uniform way of quantifying this phenotype in clinical populations, such as acute ischemic stroke (AIS) patients (Zhang et al., 2015). However, summarizing the burden on such a high level, i.e.

total WMHv, eliminates potential spatial specificity, which in turn may provide insight with regard to underlying vascular pathology and disease progression.

While other studies have explored spatial WMH patterns in diseased and healthy populations (Griffanti et al., 2017; Holland et al., 2008; Kim et al., 2008), prior studies exploring the extent of WMH on a voxel-based level in AIS patients with respect to varying risk factors, such as hypertension (Yoshita et al., 2006), were limited due to high dimensionality. For WMH, as a prototypical small vessel disease (Rost et al., 2010), a spatial differentiation may be based on supplying arteries, as previously established for stroke lesions (Ng et al., 2007). In the human brain, we distinguish between the anterior and posterior circulation. The anterior supratentorial circulation is comprised of the anterior (ACA) and middle cerebral artery (MCA), while the posterior cerebral artery (PCA) supplies the posterior supratentorial vascular area. Infratentorial structures receive their blood supply through the posterior circulation. Moreover, large-scale analysis of WMH burden for each vascular territory is limited, as manual assessment and differentiation of individual vascular territories is time consuming and results in inter-rater variations.

In general, medical image analysis is prone to inter-subject variability. It is common practice to reduce this variability by normalizing images to a common coordinate system (Mandal et al., 2012). In addition to allowing reproducible assessment of disease phenotypes across subjects with respect to their spatial location, it furthermore allows comparison across studies. Moreover, computational costs can be reduced by utilizing prior information such as brain or tissue segmentation. However, for WMH analysis in AIS patients, an age-appropriate FLAIR templates for spatial normalization in AIS populations with outlined vascular territories is currently missing.

Here, we study the distribution of WMH, differentiated by supratentorial cerebral vascular territories in clinically acquired FLAIR images of patients with AIS. In order to assess spatial distribution, we first create an age appropriate brain template, including T1, T2 and FLAIR sequences based on high-resolution MR images, and delineate all 5 bi-lateral vascular territories. We utilize these vascular territories, by spatially normalizing each subject's FLAIR image to the FLAIR template. Finally, we investigate WMHv for each of the supratentorial vascular territories with respect to the common clinical WMH risk factors, while accounting for territory size, in a generalized linear model.

2 Materials and methods

2.1 Study design and patient population.

Patients were enrolled as part of the Genes Associated with Stroke Risk and Outcomes Study (GASROS) between 2003 and 2011 (Zhang et al., 2015). Patients presenting to the Massachusetts General Hospital Emergency Department (ED) with symptoms of AIS and who were >18 years of age, were eligible to enroll. Each patient underwent standard clinical imaging protocol within 48 hours of last known well time, including T2 FLAIR imaging (TR 5000ms, minimum TE of 62 to 116ms, TI 2200ms, FOV 220-240mm). This study was carried out in accordance with the recommendations of Partners Institutional Review Board with written informed consent from all subjects. All subjects gave written informed consent in accordance with the Declaration of Helsinki. The protocol was approved by the Partners Institutional Review Board.

We identified 882 subjects with manual WMH outlines (Zhang et al., 2015) and most complete phenotypic information available for this analysis (Table 1). Manual WMH outlines were perfomed using MRIcro software for computer-assisted determination of WMHv. Maps were created using axial T2 FLAIR sequences, based on a previously published semi-automated method with high inter-rater

reliability (Chen et al., 2006). Each subjects DWI sequence was utilized to exclude acute ischemia, edema, and chronic infarcts. Additionally, 586 out of the 882 subjects had DWI lesions manually outlined, using a semi-automated algorithm (Mocking et al., 2011), by reader blinded to the admission stroke severity and 90-day outcome, measured by the modified Rankin Scale.

Table 1: Study cohort characterization. Smoking is assessed based on part or current history of smoking (ever/never).

	AIS cohort	Template cohort
n	882	16
Age (mean (sd))	65.5 (14.9)	69.6 (8.2)
Female (n (%))	337 (38.2)	6 (37.5)
Smoking (%; n missing)	561 (63.6)	5 (31.2; 4)
Hypertensive (%; n missing)	563 (63.8)	8 (50.0; 4)
WMHv (cc; mean (sd))	10.8 (13.3)	-

In addition to the AIS cohort, 16 subjects were recruited between 2016 and 2017 at Massachusetts General Hospital, to generate a high-resolution template. The template cohort selection aimed to match characteristics of elderly adults presenting to the ED with a cerebrovascular incidence in terms of age and sex. Twelve stroke-free, non-demented patients with the sporadic form of cerebral amyloid angiopathy (CAA), a known cerebral small vessel disorder and similarly-aged healthy controls (n=4) underwent high-resolution MRI as part of a separate study at our hospital (Table 1). MR scans were manually assessed to exonerate any gross pathology, such as hemorrhage or silent brain infarcts.

High-resolution structural brain MRI sequences were acquired with a Siemens Magnetom Prisma 3T scanner (using a 32-channel head coil). The standardized protocol included a Multiecho T1-weighted (voxel size: 1x1x1 mm^3; Repetition Time [TR]: 2510 ms), a 3D-FLAIR (FLAIR: voxel size: 0.9x0.9x0.9 mm^3; TR: 5000 ms; TE: 356 ms), and a T2-weighted Turbo Spin Echo (voxel size: 0.5x0.5x2.0 mm^3; TR: 7500 ms; TE: 84 ms) sequence.

2.2 Template creation

We employ Advanced Normalization Tools (ANTs) for image processing, a well-established tool for image registration and template creation (Avants et al., 2010, 2011). Utilizing the 16 high-resolution images, we create a brain template based on multimodal information using T1, T2 and FLAIR sequences. After template creation was completed, and due to the relatively low number of subjects, we smoothed the resulting templates (FSL; Gaussian smoothing, sigma = 1). Finally, we registered the resulting templates into MNI space using ANTs (Avants et al., 2011).

Additionally, manual brain extraction was performed on all subjects based on their FLAIR sequences. Binary manual masks were warped into template space and averaged. For each voxel, majority voting was performed and an average brain mask was generated based on the voxels where more than 50% of the subjects agreed. The resulting mask was manually assessed and corrected on a per-slice basis where necessary.

Vascular territories were outlined on the right hemisphere in the T1-weighted atlas image by an expert neurologist (A.K.G.). The outline was then mirrored onto the left hemisphere and subsequently combined to create a full-brain vascular territory map. This map was manually assessed and corrected where necessary. Additionally, WMHv and ventricular size were manually determined on the atlas, to ensure that the template is representative of subjects in this age category.

2.3 Neuroimage analysis of WMH burden

Each FLAIR image was first skull-stripped using an in-house skull-stripper for clinical quality scans (Schirmer et al., 2017) and then non-linearly registered to the high-resolution FLAIR template using ANTs (Avants et al., 2011). Subsequently, the vascular territory map was warped into subject space, allowing us to calculate both the volume of each vascular territory in subject space, as well as the WMH burden for each territory. Finally, we normalize each territorial WMHv by the total WMHv, to describe a relative burden per territory ($WMHv_{rel}$).

Each subject's vascular territory map is manually assessed for gross registration errors, such as midline shift. Furthermore, we identify potential outliers using the modified z-score (Iglewicz and Hoaglin, 1993) for each set of territorial volumes of the cohort. Subjects with registration errors and those deemed outliers were removed from analysis.

Additionally, we register all 586 subjects non-linearly with manual DWI lesion outlines to the FLAIR template. This allows us, with the addition of WMH outlines being mapped to the same template, to create incidence maps of both the chronic WMH disease burden, as well as the acute lesion locations.

2.4 Statistical analysis

We assess WMH burden for each territory using a generalized linear model. The model for each relative WMH burden is given by

$$WMHv_{rel} \sim Age + V_{terr} + HTN + Smoking, \quad (1)$$

including age, volume of the territory in subject space (V_{terr}), hypertensive (HTN) and smoking (ever/never) status. As a comparison, we also investigate the efficacy of this model, compared to a baseline model, where the $WMHv_{rel}$ is solely explained by V_{terr}, given by

$$WMHv_{rel} \sim V_{terr}. \qquad (2)$$

Both models are compared using a χ^2 test. Statistical analysis was conducted using the computing environment R (R Core Team, 2013).

2.5 Data availability

The utilized template will be made available upon acceptance to facilitate reproducibility of our findings. The authors agree to make available to any researcher the data, methods used in the analysis,

and materials used to conduct the research for the express purposes of reproducing the results and with the explicit permission for data sharing by the local institutional review board.

3 Results

3.1 Template and territorial map

Utilizing ANTs, we create a multimodal template from the 16 subjects with high-resolution MR images. Figure 1 shows axial slices of the T1, T2 and FLAIR template, after registration to MNI space. Additionally, it shows the vascular territory map, which was delineated on the template's T1 sequence. Within this template, WMH and ventricular volume were manually assessed, with 13.2cc and 34.4cc, respectively.

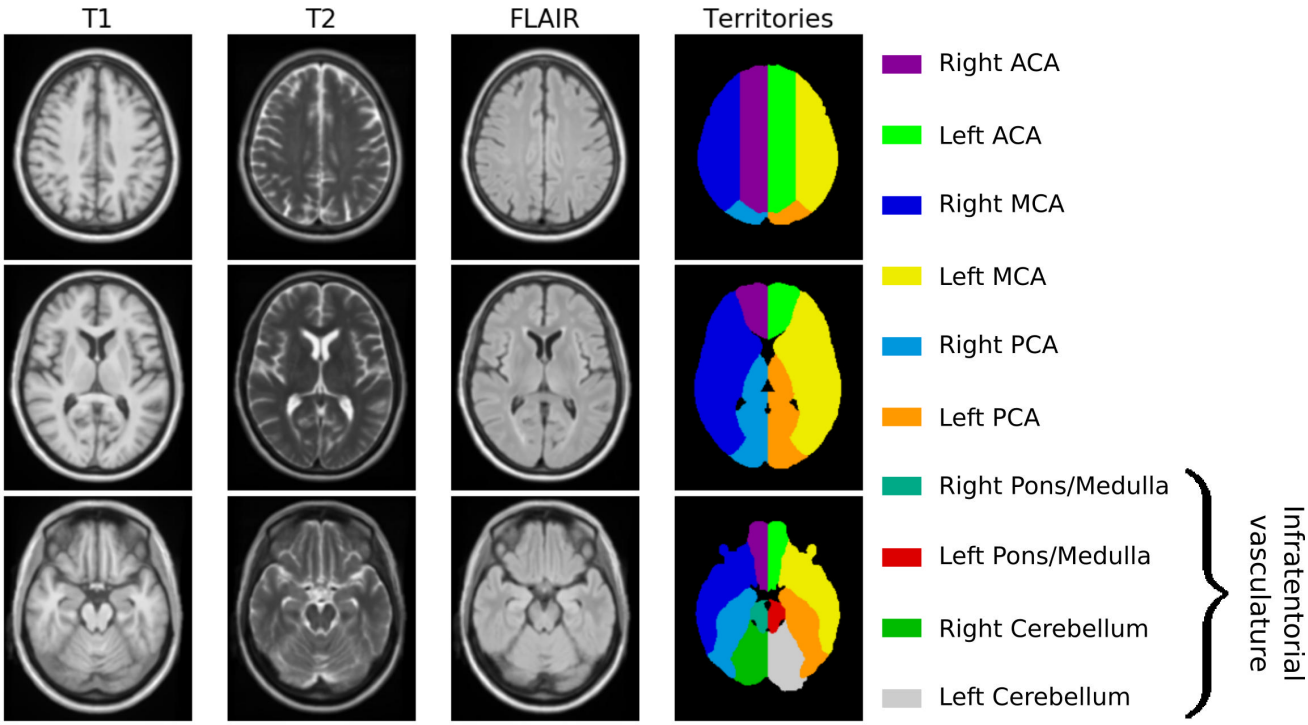

Figure 1: Age-appropriate template, including T1, T2 and FLAIR sequences for image registration, as well as vascular territory map.

3.2 Neuroimage analysis of WMH burden

Each subject is non-linearly registered to the FLAIR template and the vascular territory map transformed into low-resolution subject space. We assess each subject for registration errors, leading to 17 subjects being excluded. Utilizing the modified z-score for each territory's volumes did not lead to further exclusions. Registering the DWI volumes to the FLAIR template did not lead to any of the 586 subjects being excluded. Figure 2 shows the spatial distribution of WMH burden and acute lesion location within the template.

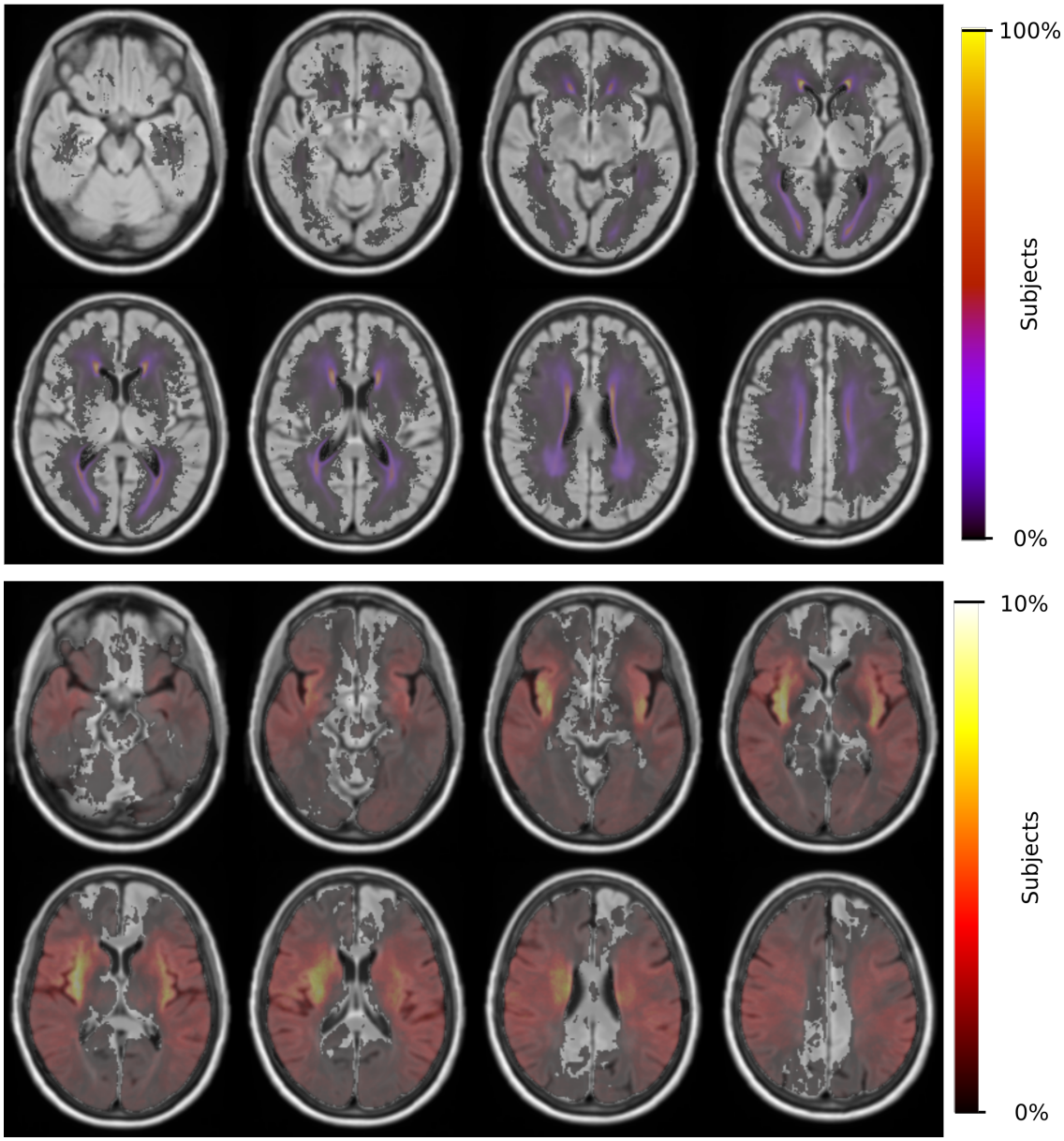

Figure 2: Distributions of WMH burden (top) and acute lesion location (bottom) for 865 patients and 586 patients, respectively.

For the remaining 865 subjects with WMH outlines, ACA, MCA and PCA volumes (mean±standard deviation) are estimated to be 334.7±40.7cc, 671.5±79.8cc and 253.9±31.9cc, respectively. WMHv within each of the bi-lateral ACA, MCA and PCA territories are calculated for each subject and normalized by the subject's total WMHv, resulting in a relative $WMHv_{rel}$ for each territory. Figure 3 shows $WMHv_{rel}$ for each vascular territory. Additionally, we combine both ACA and MCA to represent the combined anterior (ANT) territory.

We also investigate the correlations between all investigated phenotypes using Pearson's R (Table 2). We observe high positive correlations (R>0.9) between the volumes of the individual vascular territories, as well as medium negative correlations (-0.6<R<-0.4) for the relative WMH burden in each territory.

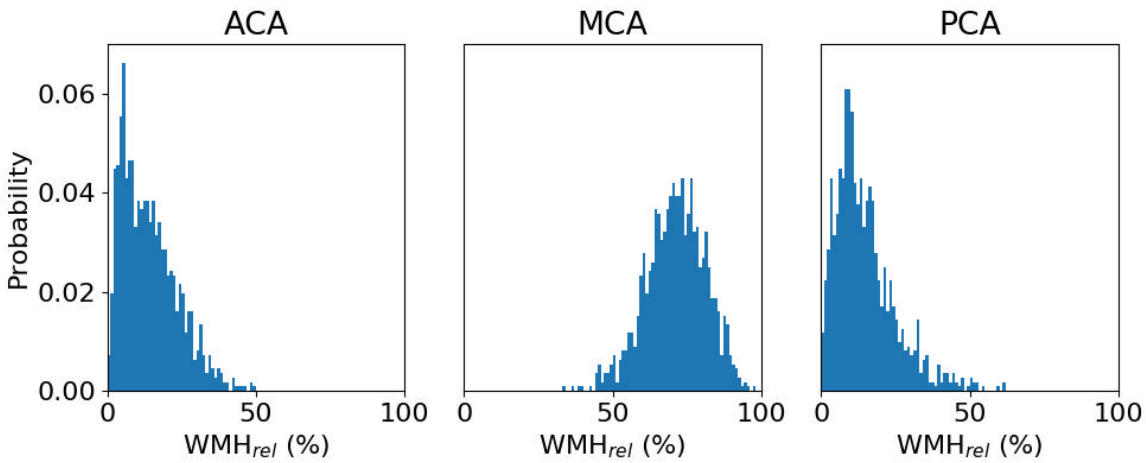

Figure 3: Distribution of relative WMH burden (WMH_{rel} (%)) for each vascular territory, with a median WMH_{rel} (interquartile range) of 13.1% (6.6%-20.7%), 70.7% (63.9%-77.5%) and 12.9% (7.8%-19.8%), respectively.

Table 2: Correlations of phenotypes (Pearson R). Statistically significant correlations (p<0.05) are shown in bold.

	$WMHv_{rel}^{ACA}$	$WMHv_{rel}^{MCA}$	$WMHv_{rel}^{PCA}$	$WMHv_{rel}^{ANT}$	V_{ACA}	V_{MCA}	V_{PCA}	V_{ANT}	Smoking	HTN
Age	**0.30**	**-0.18**	**-0.10**	**0.10**	-0.10	**-0.11**	-0.05	**-0.11**	-0.01	**0.34**
	$WMHv_{rel}^{ACA}$	**-0.45**	**-0.49**	**0.49**	-0.17	**-0.19**	**-0.09**	**-0.18**	0.03	**0.18**
		$WMHv_{rel}^{MCA}$	**-0.56**	**0.56**	-0.02	0.03	-0.04	0.01	0.06	-0.06
			$WMHv_{rel}^{PCA}$	**-1.00**	0.17	**0.14**	**0.12**	**0.15**	**-0.08**	**-0.10**
				$WMHv_{rel}^{ANT}$	**-0.17**	**-0.14**	**-0.12**	**-0.15**	**0.08**	**0.10**
					V_{ACA}	**0.94**	**0.92**	**0.97**	0.04	-0.06
						V_{MCA}	**0.94**	**0.99**	0.04	-0.06
							V_{PCA}	**0.95**	0.04	-0.04
								V_{ANT}	0.04	-0.06
									Smoking	0.02

We use the relative WMH burden as dependent variable and estimate the model parameters of the general linear model, given by equation (1). The results are summarized in Table 3 and show that age, smoking and hypertension modulate the spatial patterns of WMH burden in our cohort. In the ACA territory, age, volume of the vascular territory and hypertensive status were found statistically significant, where age and hypertensive status increase the relative burden in ACA. The only phenotype found statistically significant in MCA is age, where an increase in age is associated with the relatively lower WMH burden in MCA. All phenotypes, except for age, were found statistically significant in PCA, as well as the anterior territory, a combined ACA and MCA territory named after the "anterior" circulation versus "posterior" circulation supplied by the PCA.

Table 3: Parameter estimate for general linear model fit using R. Statistically significant parameters (p<0.05) are highlighted.

	ACA		MCA		PCA		Ant	
	Estimate (%)	p	Estimate (%)	p	Estimate (%)	p	Estimate (%)	p
Intercept	**13.449 ± 3.159**	**0.000**	**77.180 ± 3.562**	**0.000**	**9.753 ± 3.387**	**0.004**	**93.763 ± 3.642**	**0.000**
Age	**0.167 ± 0.022**	**0.000**	**-0.124 ± 0.024**	**0.000**	-0.047 ± 0.025	0.057	0.040 ± 0.025	0.106
V_{terr}	**-0.034 ± 0.008**	**0.000**	0.001 ± 0.005	0.793	**0.041 ± 0.011**	**0.000**	**-0.013 ± 0.003**	**0.000**
Smoking	0.767 ± 0.640	0.230	1.125 ± 0.702	0.109	**-1.897 ± 0.719**	**0.008**	**1.923 ± 0.717**	**0.007**
HTN	**1.561 ± 0.682**	**0.022**	-0.005 ± 0.748	0.994	**-1.555 ± 0.766**	**0.042**	**1.536 ± 0.764**	**0.044**

Comparing the models summarized in Table 3 to their corresponding baseline models given by equation (2), we find that the reduction of residual deviation of the observed data is statistically significant in each case (p<0.001).

4 Discussion

In this work we investigated the relative WMH disease burden per established cerebral vascular territory in AIS patients and how it is affected through age, smoking and hypertension – the common

vascular risk factors. To allow automated characterization of WMH burden per vascular territory, we introduced an age-appropriate template with a FLAIR sequence for registration. Both WMHv and ventricular volume of the template were representative of the disease burden in our cohort and ventricular size of found in healthy elderly (Ambarki et al., 2010). Moreover, this template allowed us to delineate vascular territories. We used this territorial map to elucidate relative spatial WMHv distributions in 865 patients with clinical FLAIR sequences, while accounting for size differences in the vascular territories.

Spatially specific effects of each investigated phenotype were identified in our cohort. Age shows a relative increase in the ACA and relative decrease in the MCA territory. There was no statistically significant change in the PCA or combined anterior territories. Whereas age is known to be one of the most robust predictors of the overall WMH burden (Zhang et al., 2015), our data suggest that a global and not spatially discriminative effect between the anterior and posterior vascular territory exists. Although we found modifying effects between ACA and MCA, the resulting unit changes are small (<0.2%/year).

Vascular territory size also modifies spatial WMH burden in ACA, PCA and the combined anterior territories; however, the effects are also small (<0.05%/cc). One possible explanation may be due to spatially specific brain atrophy. It has been shown that there is a volumetric increase in healthy controls in the ACA territory, with a decrease in the PCA territory of the brain (Cole et al., 2018). In this study, there was both volumetric increase (towards superior) and decrease (towards inferior) in the areas of the brain that composes MCA. Although AIS patients cannot be considered healthy controls, the difficulty of acquiring high-resolution brain images in this patient population due to clinical requirements of care does not allow us to investigate region specific brain atrophy patterns to correlate with the increase/decrease of relative WMH burden. Development of faster high-resolution imaging sequences, such as 3D FLAIR, may help to elucidate this relationship in future studies.

Smoking status shows the greatest modifying effect on spatially specific modifications of WMH burden with a relative increase in the combined anterior (MCA and ACA), as opposed to relative reduction of WMH in the posterior (PCA) territories. The individual effects in each of the ACA and MCA territory are similar in size, suggesting that increase in WMH burden may be spread through both territories equally; however, additional studies are required to confirm this hypothesis. In addition to smoking, hypertensive status shows an increase of relative WMH burden in the ACA and a corresponding decrease in the PCA territory. There was no effect on the MCA territory. Combining ACA and MCA into the anterior territory shows the same effect as the ACA territory, implying that the effect is driven by the spatial distribution of WMH in the ACA territory predominantly. This may be the result of the stroke lesions being predominantly in the MCA territory, thereby introducing uncertainty in identifying underlying disease burden (see Figure 2). The difference between ACA and PCA, however, may be due to differences between the small vessel architecture in both territories. However, detailed investigations into those differences are currently lacking.

There are some limitations to our study. In general, spatial normalization of clinical low-resolution images is a non-trivial task, in particular in AIS patients, where biological responses to the stroke, such as mass effects, can play an important role. In this study, we manually assessed the registration, leading to 17 subjects being excluded from final analysis due to gross registration errors. Nonetheless, small registration errors may be important for assessing WMHv within vascular territories. However, using an age-appropriate FLAIR template is a first step to mitigate the resulting uncertainties. Although we demonstrated spatially discriminative changes of relative WMH burden, the underlying etiology needs to be further elucidated. This, however, requires additional investigation into the capillary densities

and networks of each vascular territory and is beyond the scope of this work. Other types of analyses will also be considered in future work. One promising, hypothesis free approach is the use of voxel-based lesion symptom mapping. While such analysis may reveal interesting correlates of the presentation of WMH in our cohort, its hypothesis free nature makes it difficult to directly interpret the results. By relying on a hypothesis-driven approach in this analysis, however, we are able to attribute the WMH burden to the individual supplying arteries.

In this work, we demonstrated that the vascular risk factors such as hypertension and smoking status influence spatial specificity of WMH, one of the most important radiographic manifestations of chronic cerebral ischemia. Here, we illustrated that WMH burden does not develop homogeneously throughout the supratentorial brain. These findings of spatial specificity of WMH in relation to vascular territory and risk factor exposure in AIS patients open the path for new investigations into underlying pathology of this common vascular disease and its associated risk factors, and ultimately into its connection with stroke.

Acknowledgements

This project has received funding from the European Union's Horizon 2020 research and innovation programme under the Marie Sklodowska-Curie grant agreement No 753896 (M.D. Schirmer). This study was supported by the NIH–National Institute of Neurological Disorders and Stroke (K23NS064052, R01NS082285, and R01NS086905), American Heart Association/Bugher Foundation Centers for Stroke Prevention Research, and Deane Institute for Integrative Study of Atrial Fibrillation and Stroke.

Author contributions

All authors had full access to all the data in the study and take responsibility for the integrity of the data and the accuracy of the data analysis. *Conceptualization*, MS, AG, OW, NR; *Methodology*, MS and NR; *Investigation*, MS, AG, PF, ME, LC, AV, SG, OW and NR; *Formal Analysis*, MR; *Writing – Original Draft*, MS and NS; *Writing – Review & Editing*, MS, AG, PF, ME, LC, AV, SG, OW and NR; *Visualization*, MS; *Supervision*, NR;

Conflict of interest statements

The authors report no conflicts of interest.

References

Ambarki, K., Israelsson, H., Wahlin, A., Birgander, R., Eklund, A., and Malm, J. (2010). Brain ventricular size in healthy elderly: comparison between Evans index and volume measurement. *Neurosurgery* 67, 94–99.

Avants, B. B., Tustison, N. J., Song, G., Cook, P. A., Klein, A., and Gee, J. C. (2011). A reproducible evaluation of ANTs similarity metric performance in brain image registration. *Neuroimage* 54, 2033–2044.

Avants, B. B., Yushkevich, P., Pluta, J., Minkoff, D., Korczykowski, M., Detre, J., et al. (2010). The optimal template effect in hippocampus studies of diseased populations. *Neuroimage* 49, 2457–2466.

Chen, Y. W., Gurol, M. E., Rosand, J., Viswanathan, A., Rakich, S. M., Groover, T. R., et al. (2006). Progression of white matter lesions and hemorrhages in cerebral amyloid angiopathy. *Neurology* 67, 83–87.

Cole, J. H., Jolly, A., de Simoni, S., Bourke, N., Patel, M. C., Scott, G., et al. (2018). Spatial patterns of progressive brain volume loss after moderate-severe traumatic brain injury. *Brain*.

Debette, S., and Markus, H. S. (2010). The clinical importance of white matter hyperintensities on brain magnetic resonance imaging: systematic review and meta-analysis. *Bmj* 341, c3666.

Giese, A.-K., Schirmer, M. D., Donahue, K. L., Cloonan, L., Irie, R., Winzeck, S., et al. (2017). Design and rationale for examining neuroimaging genetics in ischemic stroke The MRI-GENIE study. *Neurol. Genet.* 3, e180.

Griffanti, L., Jenkinson, M., Suri, S., Zsoldos, E., Mahmood, A., Filippini, N., et al. (2017). Classification and characterization of periventricular and deep white matter hyperintensities on MRI: a study in older adults. *NeuroImage*.

Holland, C. M., Smith, E. E., Csapo, I., Gurol, M. E., Brylka, D. A., Killiany, R. J., et al. (2008). Spatial distribution of white-matter hyperintensities in Alzheimer disease, cerebral amyloid angiopathy, and healthy aging. *Stroke* 39, 1127–1133.

Iglewicz, B., and Hoaglin, D. C. (1993). *How to detect and handle outliers*. ASQC Quality Press Milwaukee, WI.

Kim, K. W., MacFall, J. R., and Payne, M. E. (2008). Classification of white matter lesions on magnetic resonance imaging in elderly persons. *Biol. Psychiatry* 64, 273–280.

Kuller, L. H., Longstreth, W. T., Arnold, A. M., Bernick, C., Bryan, R. N., and Beauchamp, N. J. (2004). White matter hyperintensity on cranial magnetic resonance imaging: a predictor of stroke. *Stroke* 35, 1821–1825.

Mandal, P. K., Mahajan, R., and Dinov, I. D. (2012). Structural brain atlases: design, rationale, and applications in normal and pathological cohorts. *J. Alzheimers Dis.* 31, S169–S188.

Mocking, S., Garg, P., Chutinet, A., Copen, W., Sorensen, A., and Wu, O. (2011). Accuracy and execution speed of automatic voxel-based algorithms for segmenting stroke lesions in clinical DWI imaging (abstract). in.

Ng, Y. S., Stein, J., Ning, M., and Black-Schaffer, R. M. (2007). Comparison of clinical characteristics and functional outcomes of ischemic stroke in different vascular territories. *Stroke* 38, 2309–2314.

R. Core Team (2013). R: A language and environment for statistical computing.

Rost, N. S., Rahman, R. M., Biffi, A., Smith, E. E., Kanakis, A., Fitzpatrick, K., et al. (2010). White matter hyperintensity volume is increased in small vessel stroke subtypes. *Neurology* 75, 1670–1677.

Schirmer, M. D., Dalca, A. V., Sridharan, R., Giese, A.-K., Broderick, J., Jimenez-Conde, J., et al. (2017). Fully automated pipeline for white matter hyperintensity segmentation using clinical scans in patients with acute ischemic stroke (S19. 001). *Neurology* 88, S19. 001.

Yoshita, M., Fletcher, E., Harvey, D., Ortega, M., Martinez, O., Mungas, D. M., et al. (2006). Extent and distribution of white matter hyperintensities in normal aging, MCI, and AD. *Neurology* 67, 2192–2198.

Zhang, C. R., Cloonan, L., Fitzpatrick, K. M., Kanakis, A. S., Ayres, A. M., Furie, K. L., et al. (2015). Determinants of white matter hyperintensity burden differ at the extremes of ages of ischemic stroke onset. *J. Stroke Cerebrovasc. Dis.* 24, 649–654.